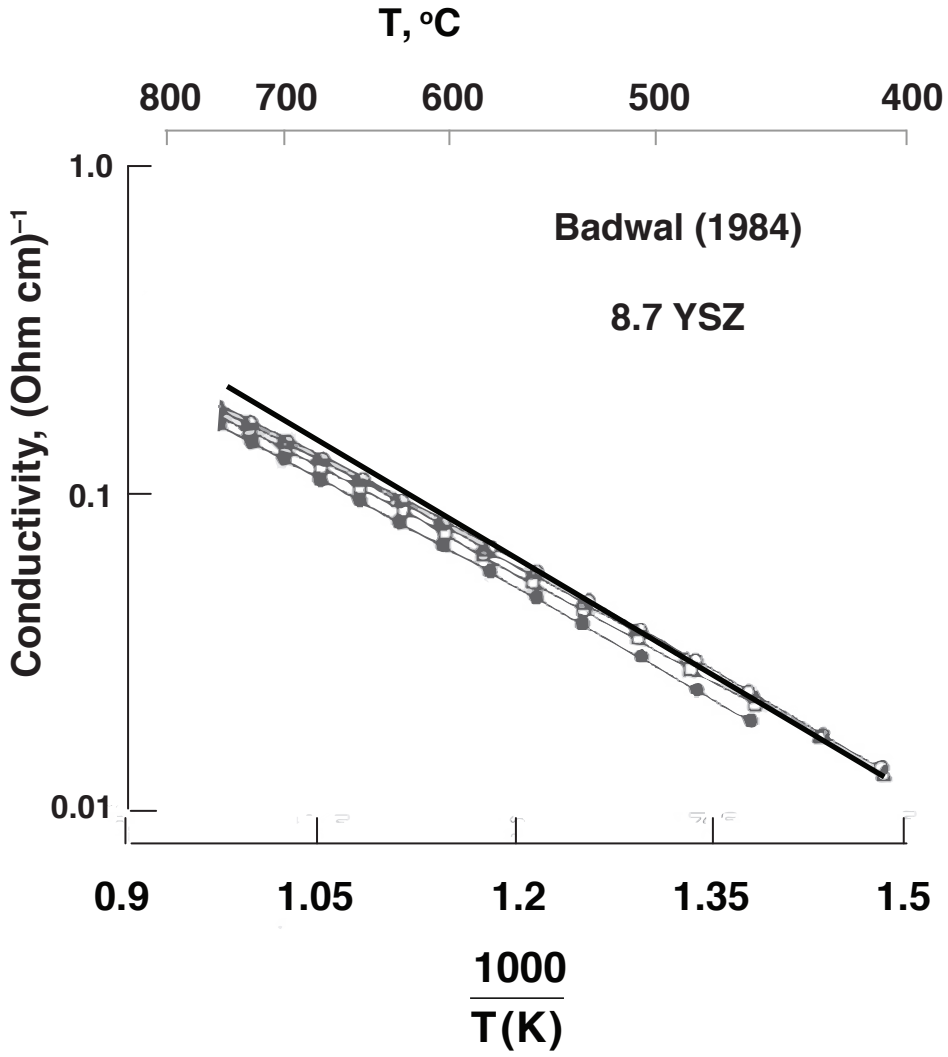
T, °C
800
700
600
500
400
1.0
0.1
0.01
Conductivity, (Ohm cm)⁻¹
Badwal (1984)
8.7 YSZ
0.9
1.05
1.2
1.35
1.5
1000
T(K)

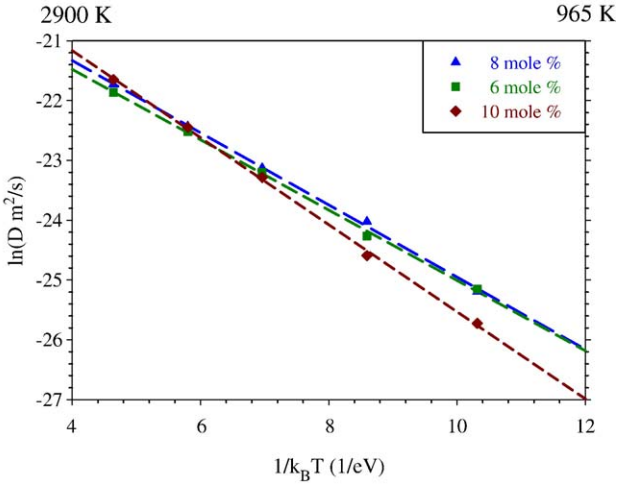

Fig. 7. Arrhenius plot of the diffusion coefficient as a function of reciprocal temperature ($1/T$) for 6 (■), 8(▲), and 10(◆) mol% YSZ. Linear fits to the data are also shown.

obtained for projections along the x- and z-axes, which indicate that the oxygen ion transport occurs along [001].

Fig. 7 is an Arrhenius plot (Eq. (3)) of D vs. $(1/k_BT)$ for oxygen migration in 6, 8 and 10 mole % YSZ. The data points are from the present MD simulations for a period of 2 to 5 ns at 1125, 1350, 1667, 2000 and 2500 K. The lines are the best fit to the data according to Eq. (3). The slope gives the activation energy for oxygen migration, and the intercept the pre-exponent. We find that the diffusion coefficient is highest at 8 mole % YSZ, consistent with experimental results [3,4]. The data points for 12, 15, 18 and 25 mole % Y_2O_3 are not shown for the sake of clarity. Above 10 mole % Y_2O_3, the diffusion coefficient decreased with increasing yttria content.

The activation energy for oxygen migration in YSZ is shown as a function of composition in Fig. 8. The plot is on the same scale as Figs. 1 and 2 to facilitate comparison with published data. The activation energy (ΔH_m) shows an upward trend with

Table 1
Pre-exponent (D_0) and activation energy (ΔH) for oxygen diffusion in YSZ

Mole % Y_2O_3	D_0 (10^{-9} m^2/s)	ΔH (eV)	D (m^2/s) at 1273 K
6	4.94	0.59	2.28×10–11
8	6.08	0.60	2.56×10–11
10	11.81	0.73	1.52×10–11
11	12.62	0.75	1.30×10–11
12	12.59	0.76	1.24×10–11
15	20.03	0.86	0.79×10–11
18	11.01	0.82	0.62×10–11
25	20.48	0.98	0.27×10–11

increasing Y_2O_3 content. The best linear fit is also shown and has the form;

$$\Delta H_m(\text{eV}) = 0.5 + 0.02y, \tag{6}$$

where y is the yttria mole % (in the range 6 to 25%). Activation energies obtained in the present work are about 0.2 eV below the experimental data ($\Delta H_m + \Delta H_a$) of Ioffe et al [3] shown in Fig. 1. Since ΔH_a is estimated to be about 0.1–0.2 eV [28], we consider our data to be in agreement with the values of Ioffe et al [3] and the general experimental trend of increasing activation energies with increasing mole % of Y_2O_3. Our data also show good agreement with the values reported by Pornprasertsuk et al [23] based on first principles calculations.

D_0 and ΔH_m are listed in Table 1 along with D at a typical SOFC operating temperature (1273 K) for all the YSZ compositions studied. By determining these values using molecular dynamics, we have implicitly included ionic environment effects that are often left out in static calculations of barrier heights that consider mainly first neighbor effects. We find that the overall trend is that both D_0 and ΔH_m increase with the increasing mole % of Y_2O_3. As the Y_2O_3 content increases, the vacancy concentration increases, leading to an increase in D_0. However, the increase of D due to this effect is countered by an increase in ΔH_m. It appears that the balance between these two effects is reached at around 8 mole % YSZ as shown by the last column in Table 1.

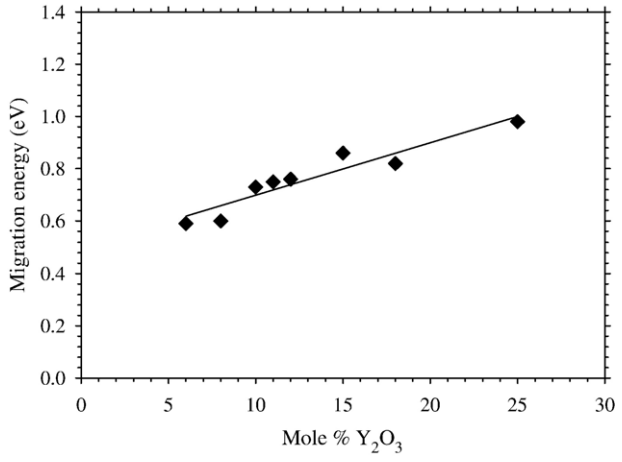

Fig. 8. Activation energy for oxygen migration in YSZ as a function of composition along with a linear fit to the data.

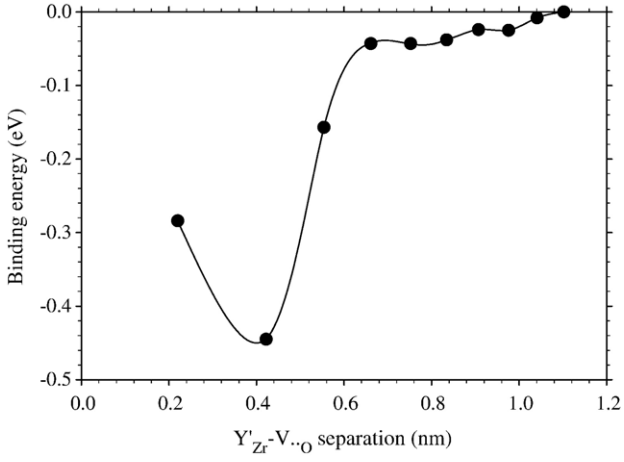

Fig. 9. Dopant–vacancy binding energy in YSZ as a function of separation. Lines connecting the data points are shown to guide the eye.

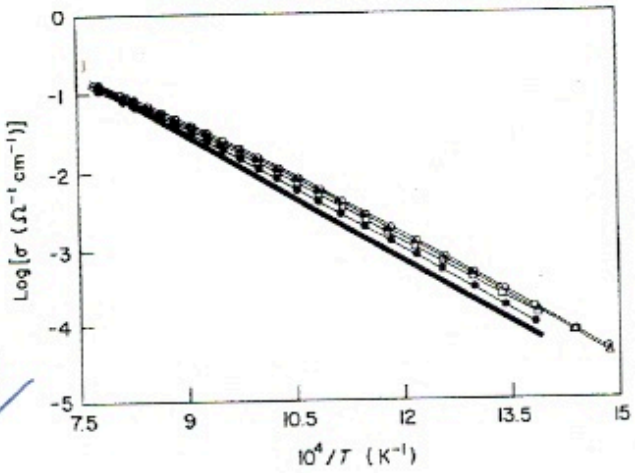

Figure 4 Arrhenius plots for the d.c. conductivity of various polycrystalline samples. ○, B1; △, C1; □, D1; ●, E1.

the sake of convenience and clarity also expressed as conductivities, are plotted in Fig. 8. The agreement between the four-probe d.c. data and the total conductivity as measured by the complex impedance technique was reasonably good. After separation of the grain boundary contribution, the volume conductivities of all the samples from series B to E were identical. The grain boundary resistance was relatively small in the purest polycrystalline samples and it increased from series B to D. During preparation of the samples for series C and D, Y_2O_3 and ZrO_2 powders were mixed zirconia) balls which contained impurities such as SiO_2 (~0.4 wt %). Thus minor impurity contamination is possible and it, in addition to the grain size effect obvious in Fig. 1, may also have contributed to the higher grain boundary resistance of these samples.

The greatest contribution to the grain boundary resistance was observed for samples form series E and F which contained deliberately added impurity (1 wt % SiO_2). Heat treatment of the samples from series F at 1700° C (series E) resulted in decreases in both the grain boundary and the volume resistance, although it was the grain boundary arc which was the more strongly affected (Fig. 5d and e). The minor increase in the volume conductivity is probably due to the increased density of sample E2 achieved by high-temperature sintering.

In general, the grain boundary resistance increased with decrease in the grain size and increase in the porosity (Figs. 1, 5 and 8). It also increased with impurity level and is more obvious in samples from series D and E both of which appear to have a similar grain size distribution but significantly different grain boundary resistance.

4.2.2. Single-crystal samples

Single crystal Y_2O_3–ZrO_2 samples gave one arc in the complex impedance plane, due to the lattice conductivity, over the entire temperature range (Fig. 9). However, below about 400° C the arc became slightly distorted on the low frequency side. The distortion was least for the transparent single crystal. A similar phenomenon is evident in

TABLE II D.C. resistivities of various samples at several temperatures

Sample	d.c. resistivity* (Ω cm)*					
	T(° C)					
	1000	800	700	600	500	450
A1†	–	25.1	57.1	208	1190	3615
A1	8.67	36.2	97.5	356	1975	5730
B1	8.41	32.3	93.8	351	2050	6530
C1	8.63	35.2	96.6	376	2195	6700
D1	9.04	38.0	105.7	405	2405	7415
E1	9.68	43.2	126.8	512	3230	10235

*Cooling cycle data except for A1†.
†First heating cycle data (transparent single crystal).

Badwal 1984

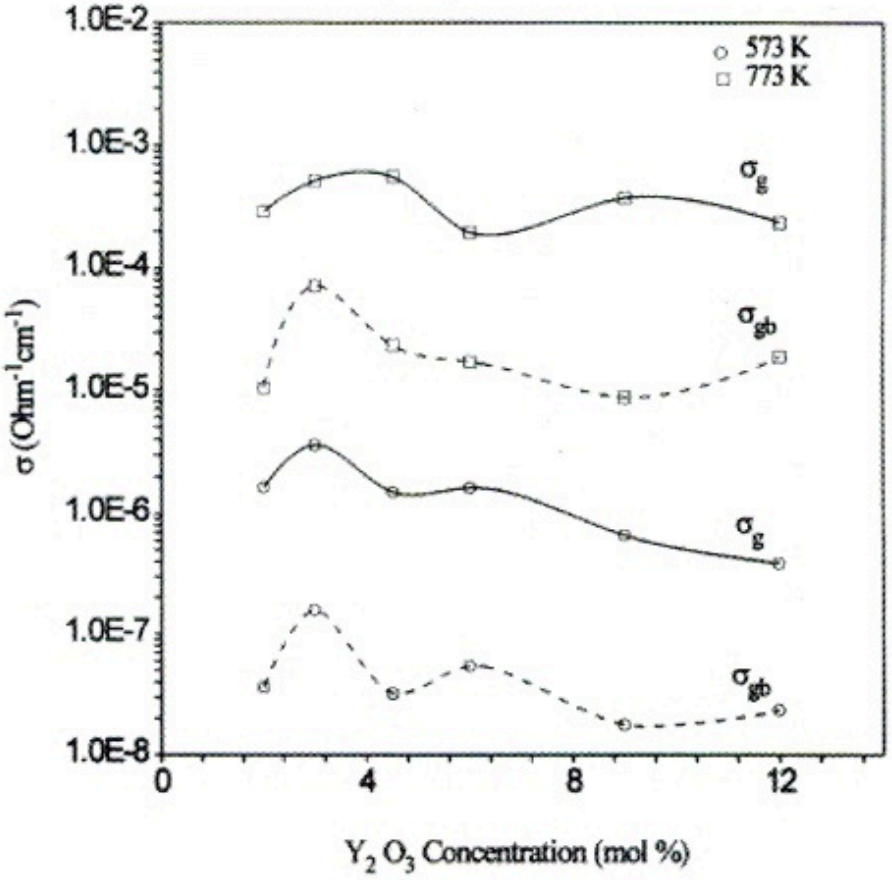

H-G Scott

J. Mater-Sci

10 (1975) 1527+535